Acta Neurochirurgica (2019) 161:1919–1929
https://doi.org/10.1007/s00701-019-03993-3

ORIGINAL ARTICLE - NEUROSURGICAL ANATOMY

# Endoscopic transorbital approach to anterolateral skull base through inferior orbital fissure: a cadaveric study

Bon-Jour Lin[1,2] · Da-Tong Ju[1] · Tzu-Hsien Hsu[1,3] · Tzu-Tsao Chung[1] · Wei-Hsiu Liu[1] · Dueng-Yuan Hueng[1] · Yuan-Hao Chen[1] · Chung-Ching Hsia[1] · Hsin-I Ma[1] · Ming-Ying Liu[1] · Hung-Chang Hung[4,5] · Chi-Tun Tang[1]

Received: 20 April 2019 / Accepted: 25 June 2019 / Published online: 29 June 2019


## Abstract

**Background** Endoscopic transorbital approach (eTOA) has been announced as an alternative minimally invasive surgery to skull base. Owing to the inferior orbital fissure (IOF) connecting the orbit with surrounding pterygopalatine fossa (PPF), infratemporal fossa (ITF), and temporal fossa, the idea of eTOA to anterolateral skull base through IOF is postulated. The aim of this study is to access its practical feasibility.

**Methods** Anatomical dissections were performed in five human cadaveric heads (10 sides) using 0-degree and 30-degree endoscopes. A stepwise description of eTOA to anterolateral skull base through IOF was documented. The anterosuperior corner of the maxillary sinus in the horizontal plane of the upper edge of zygomatic arch was defined as reference point (RP). The distances between the RP to the foramen rotundum (FR), foramen ovale (FO), and Gasserian ganglion (GG) were measured. The exposed area of anterolateral skull base in the coronal plane of the posterior wall of the maxillary sinus was quantified.

**Results** The surgical procedure consisted of six steps: (1) lateral canthotomy with cantholysis and preseptal lower eyelid approach with periorbita dissection; (2) drilling of the ocular surface of greater sphenoid wing and lateral orbital rim osteotomy; (3) entry into the maxillary sinus and exposure of PPF and ITF; (4) mobilization of infraorbital nerve with drilling of the infratemporal surface of the greater sphenoid wing and pterygoid process; (5) exposure of middle cranial fossa, Meckel's cave, and lateral wall of cavernous sinus; and (6) reconstruction of orbital floor and lateral orbital rim. The distances measured were as follows: RP-FR = 45.0 ± 1.9 mm, RP-FO = 55.7 ± 0.5 mm, and RP-GG = 61.0 ± 1.6 mm. In comparison with the horizontal portion of greater sphenoid wing, the superior and inferior axes of the exposed area were 22.3 ± 2.1 mm and 20.5 ± 1.8 mm, respectively. With reference to the FR, the medial and lateral axes of the exposed area were 11.6 ± 1.1 mm and 15.8 ± 1.6 mm, respectively.

**Conclusions** The eTOA through IOF can be used as a minimally invasive surgery to access whole anterolateral skull base. It provides a possible resolution to target lesion involving multiple compartments of anterolateral skull base.

**Keywords** Endoscopic transorbital · Inferior orbital fissure · Anterolateral skull base

This article is part of the Topical Collection on *Neurosurgical Anatomy*

✉ Chi-Tun Tang
coleman0719@gmail.com

[1] Department of Neurological Surgery, Tri-Service General Hospital, National Defense Medical Center, No. 325, Section 2, Cheng-Kung Road, Neihu, 114 Taipei, Taiwan, Republic of China

[2] Department of Surgery, Nantou Hospital, Nantou, Taiwan, Republic of China

[3] Department of Surgery, Taichung Armed Forces General Hospital, Taichung, Taiwan, Republic of China

[4] Department of Internal Medicine, Nantou Hospital, Nantou, Taiwan, Republic of China

[5] Department of Healthcare Administration, Central Taiwan University of Science and Technology, Taichung, Taiwan, Republic of China

## Introduction

Anterolateral skull base, including pterygopalatine fossa (PPF), infratemporal fossa (ITF), middle cranial fossa (MCF), and Meckel's cave, is difficult to approach due to its deep location and nearby complex neurovascular structures. Transcranial approaches to anterolateral skull base are time-consuming tasks with a high risk of cosmetic disfiguration and operative morbidity secondary to brain retraction and damage of critical structures en route to the target [16, 19, 24, 29, 31]. Accompanying with the rapid development of endoscopic skull base surgery, several reports have proved the clinical feasibility and safety of the endoscopic endonasal approach as a minimally invasive surgical trajectory to PPF, IFT, MCF, and Meckel's cave [10, 18, 21, 28, 30, 33].

The endoscopic endonasal approaches use the sinonasal tract as a natural corridor to reach the paramedian skull base, and the endoscopic endonasal transmaxillary transpterygoid approach is the most commonly used. Extensive bone drilling and dissection near the cavernous sinus and internal carotid artery, sacrifice and transposition of the contents of PPF and ITF, and limited area of exposure are major disadvantages of endonasal route to anterolateral skull base.

In recent years, the endoscopic transorbital approach (eTOA) has been announced as an alternative minimally invasive surgery to anterior and middle cranial fossae [2, 8, 12, 20, 22, 27]. The main advantage of eTOA is providing a short and straight pathway to paramedian skull base without brain retraction and obvious ophthalmologic complications [27]. Due to its novelty and possibility, several cadaveric studies have paid attention to expanded application of eTOA for different targets of interest [3, 6, 7, 13, 15]. The inferior orbital fissure (IOF) is a narrow space lying along the inferolateral quadrant of the orbit in an anterolateral direction and separating the lateral wall of orbit from the orbital floor. The length of IOF is divided into three segments, including posteromedial, middle, and anterolateral segments [9] (Fig. 1a). Each segment of IOF has a connecting corridor between the orbit and surrounding fossa (Fig. 1b). Because of its anatomical relationship, the authors postulate that eTOA through IOF can reach anterolateral skull base surrounding the orbit, including PPF, ITF, MCF, and Meckel's cave, simultaneously. The aim of this study is to access the practical feasibility of eTOA to anterolateral skull base through IOF. The surgical procedure and related anatomical landmarks are described in a stepwise manner.

## Methods

Anatomical dissections were performed in the Skull Base Laboratory at the National Defense Medical Center with five formalin-fixed, silicon-injected adult cadaveric heads (10 sides). The whole procedures were executed by a three-hand technique and using neurosurgical endoscopic instruments. The rigid 4-mm-diameter, 18-cm-length, and 0-degree and 30-degree endoscopes (Karl Storz, Tuttlingen, Germany), coupled with a high-definition camera and a digital video recorder system (Karl Storz), were used for image acquisition. A stepwise endoscopic dissection of the eTOA to anterolateral skull base through IOF was illustrated.

The IOF was a narrow and elongated space located between the lateral wall of orbit and the orbital floor. It was bounded anteriorly by the orbital surface of maxilla, posteriorly by the ocular surface of greater sphenoid wing (GSW), laterally by the orbital surface of zygomatic bone, and medially by the orbital process of palatine bone. The whole length of IOF was divided into posteromedial, middle, and anterolateral segments (Fig. 1a). In the posteromedial segment of IOF, the orbit communicated with the PPF. The middle and anterolateral segments of IOF provided pathways from the orbit to the temporal fossa and ITF, respectively (Figs. 1b and 2). In this study, the bony structure forming the lateral two thirds of the IOF was scheduled to remove as wide as possible for enlarging the corridors between the orbit and surrounding fossae. Three stages of bony drilling constituted the cornerstone of this approach: (1) drilling of the ocular surface of GSW and lateral orbital rim osteotomy, (2) removal of maxilla surrounding IOF including orbital surface lateral to the infraorbital groove, posterior and lateral walls of the maxillary sinus, and (3) drilling of the infratemporal surface of GSW and pterygoid process (Fig. 3). The anterosuperior corner of the maxillary sinus in the horizontal plane of the upper edge of zygomatic arch was defined as the reference point within this study. The distances between the reference point and anatomic landmarks, including the anterior

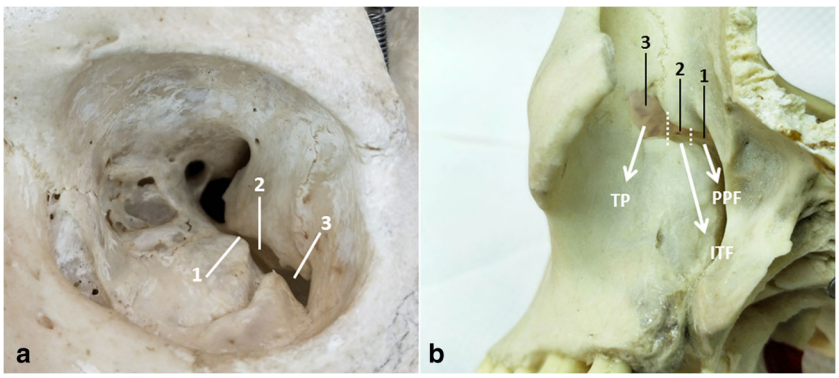


**Fig. 1** Photograph of the left orbit describing the osseous anatomy of the inferior orbital fissure (IOF) and surrounding fossae. **a** Anterior view of the three segments of IOF. Posteromedial segment (1), from the maxillary strut to the medial border of the infraorbital groove (IOG). Middle segment (2), the width of the infraorbital IOG at the IOF. Anterolateral segment (3), from the lateral border of the IOG to the anterolateral corner of the IOF. **b** Posterolateral view of the three segments of IOF. The IOF was the gateway from the orbit to the anterolateral skull base, including pterygopalatine fossa (PPF), infratemporal fossa (ITF), and temporal fossa (TF). The middle cranial fossa, separated by the greater sphenoid wind, is located behind the orbit

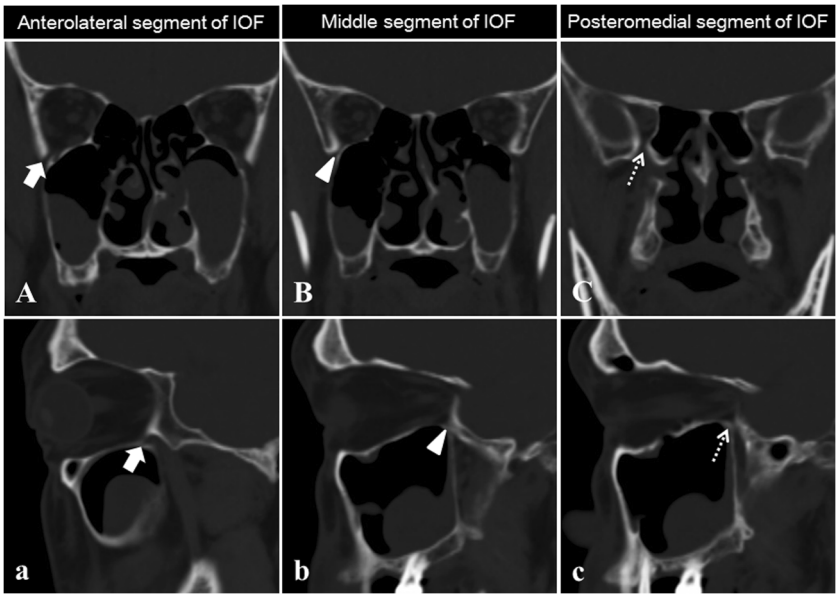


**Fig. 2** Coronal and sagittal computed topography (CT) images illustrating the communications between the orbit and surrounding fossae through the inferior orbital fissure (IOF). **A**, **a** CT images through the anterolateral segment of IOF. Arrow indicates the communication between the orbit and temporal fossa. **B**, **b** CT images through the middle segment of IOF. Arrowhead indicates the communication between the orbit and the infratemporal fossa. **C**, **c** CT images through the posteromedial segment of IOF. Arrow with dashed line indicates the communication between the orbit and the pterygopalatine fossa

margin of foramen rotundum, the anterior margin of foramen ovale, and the anterior margin of Gasserian ganglion, defined as the anterior junction of maxillary nerve and mandibular nerve, were measured. The working space for approaching PPF and ITF was a triangle consisting of three points: reference point, anterior margin of foramen rotundum, and infraorbital foramen where the orbitomaxillary segment of the infraorbital nerve connected with the cutaneous segment (Fig. 4a, d). The area of triangle was calculated by measuring the distance between each point and using Heron's formula.

The area of exposure was defined as the exposed anterolateral skull base in the coronal plane of the posterior wall of the maxillary sinus. The vertical line passing through the foramen rotundum and the horizontal portion of greater sphenoid wing were used as the longitudinal and horizontal references to define the exposed area. The extent of exposure in each axis was recorded (Fig. 4a).

## Results

The eTOA to anterolateral skull base through IOF was composed of six steps: (1) lateral canthotomy with cantholysis and preseptal lower eyelid approach with periorbita dissection; (2) drilling of the ocular surface of GSW and lateral orbital rim osteotomy; (3) entry into the maxillary sinus and exposure of the PPF and ITF; (4) mobilization of the infraorbital nerve (ION) with drilling of the infratemporal surface of GSW and pterygoid process; (5) exposure of MCF, Meckel's cave, and

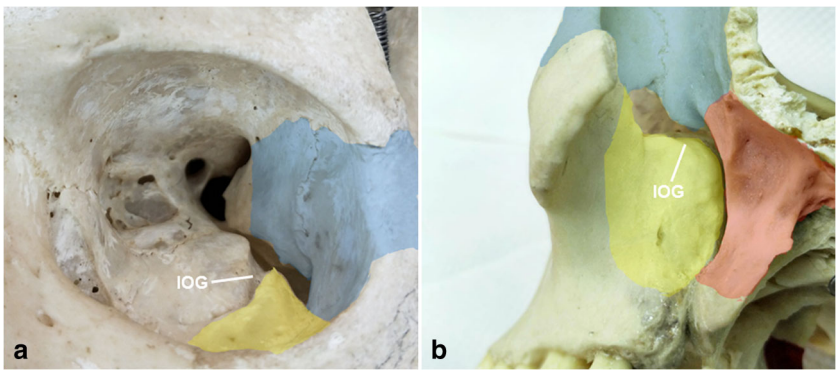


**Fig. 3** Anterior view (**a**) and posterolateral view (**b**) of the left orbit depicting the three stages of bone drilling. Stage 1 (blue-shaded area), drilling of the ocular surface of greater sphenoid wing and lateral orbital rim osteotomy (blue-shaded area) for widening the lateral two thirds of inferior orbital fissure (IOF) superior and laterally. Stage 2 (yellow-shaded area), removal of maxilla surrounding the IOF, including the orbital surface lateral to the infraorbital groove, posterior and lateral walls of the maxillary sinus, for widening lateral two thirds of IOF inferiorly and laterally. Stage 3 (red-shaded area), drilling of the infratemporal surface of the greater sphenoid wing and pterygoid process

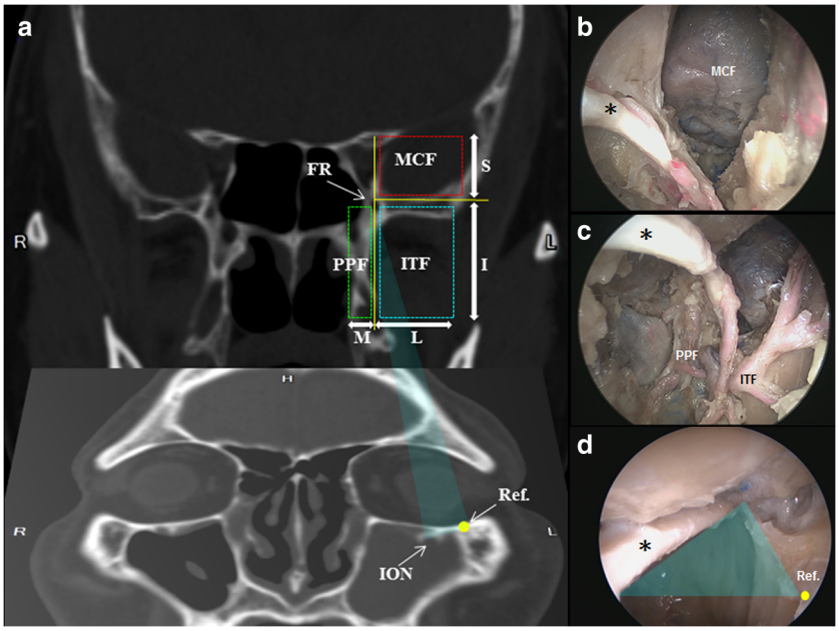


**Fig. 4** Image description of endoscopic transorbital approach to anterolateral skull base through inferior orbital fissure. **a** Coronal computed tomography images were used to illustrate the surgical planning. The antero-superior corner of the maxillary sinus in the horizontal plane of the upper edge of zygomatic arch was defined as the reference point. Reference point, foramen rotundum (FR), and the location where the infraorbital nerve (ION) entering the infraorbital foramen established the working area (blue triangle) for dissection of pterygopalatine fossa (PPF) and infratemporal fossa (ITF). The vertical line passing through the FR and horizontal portion of greater sphenoid wing formed the longitudinal and horizontal reference to define the exposed area of anterolateral skull base. The extent of exposure in each axis was recorded. **b** Middle cranial fossa was superolateral to the ION (asterisk) passing through the FR. **c** PPF was inferomedial to the ION (asterisk) passing through FR, and ITF was inferolateral. **d** Photography of working area (blue triangle) for dissection of PPF and ITF. *I* inferior axis; *L* lateral axis; *M* medial axis; *Ref.* reference point; *S* superior axis

lateral wall of cavernous sinus; and (6) reconstruction of orbital roof and lateral orbital rim.

## Lateral canthotomy with cantholysis and preseptal lower eyelid approach with periorbita dissection

Lateral canthotomy and cantholysis were performed with a 2-cm straight incision, starting at the lateral canthus and extending laterally, and cutting the superior and inferior cruxes of lateral canthus tendon (Fig. 5a). The lateral orbital rim was exposed from the fronto-zygomatic suture superiorly to the level of zygomatic arch inferiorly (Fig. 5b). The inferior orbital rim and inferolateral corner was revealed by the conjunctival incision and inferior lower eyelid approach (Fig. 5c) [25]. The periosteum was incised and left off the orbital rim to expose the orbital floor and IOF (Fig. 5d).

## Drilling of the ocular surface of GSW and lateral orbital rim osteotomy

The periorbita over the anterolateral segment of IOF was incised to expose the ocular surface of GSW (Fig. 6b). The periorbita was then elevated circumferentially along the inner aspect of orbital wall toward the orbital apex. The anatomical landmarks of dissection were the meningo-orbital band, located over the lateral aspect of superior orbital fissure, and the infraorbital nerve, located over the middle segment of IOF (Fig. 6c). Drilling of the ocular surface of GSW started from lateral to medial and underwent from anterior to posterior. Superior orbital fissure was the upper limit of drilling, and the horizontal portion of GSW was the lower limit (Fig. 6e, f). Temporalis muscle was the lateral boundary. The imaginary line, connecting the lateral aspect of superior orbital fissure and the middle segment of IOF, formed the medial boundary of the ocular surface of GSW drilling. After completing bone drilling, the lateral orbital rim osteotomy was performed by cutting the orbital rim at the level of fronto-zygomatic suture, and an inferior bone cut was made at the level of the upper edge of zygomatic arch.

## Entry into the maxillary sinus and exposure of PPF and ITF

This stage started from identification of the orbitomaxillary segment of ION coursing within the

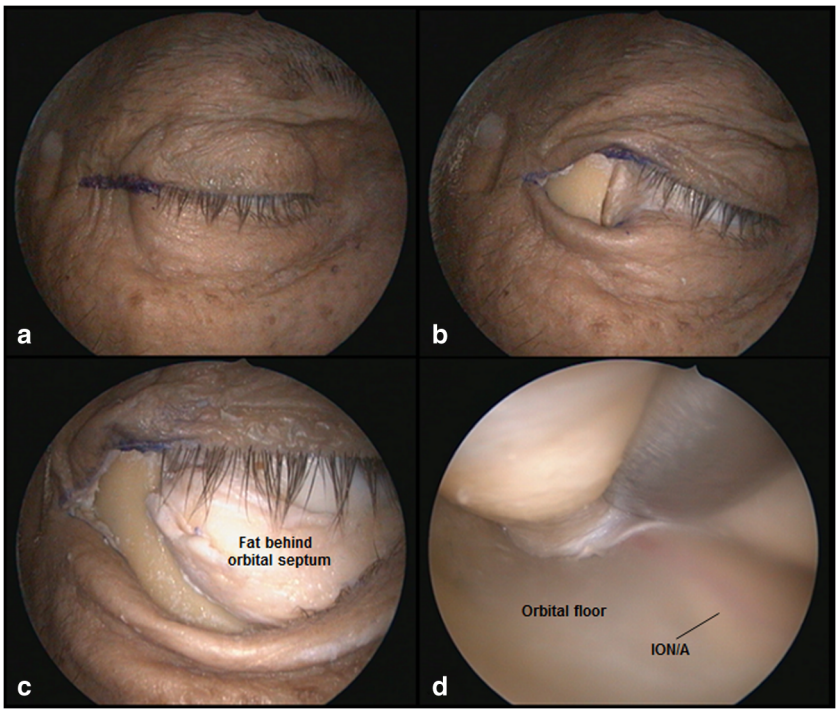


**Fig. 5** Demonstration of the endoscopic transorbital approach to anterolateral skull base (right side). **a** A linear skin incision (blue line) was cut along the natural skin crease of lateral canthus. **b** After performing lateral cantholysis, the periosteum was dissected to expose the lateral orbital rim. **c** Preseptal lower eyelid approach was performed to reveal the inferior orbital rim, where periosteum was incised to identify the dissection plane between the periorbita and the orbital floor **d** Orbit was retracted superiorly to see the anterolateral segment of inferior orbital fissure and infraorbital nerve along with infraorbital artery (ION/A) coursing beneath the orbital floor

infraorbital groove and infraorbital canal (Fig. 7a). The orbital floor located between the orbitomaxillary segment of ION and the lateral wall of the maxillary sinus was removed in a medial-to-lateral direction to

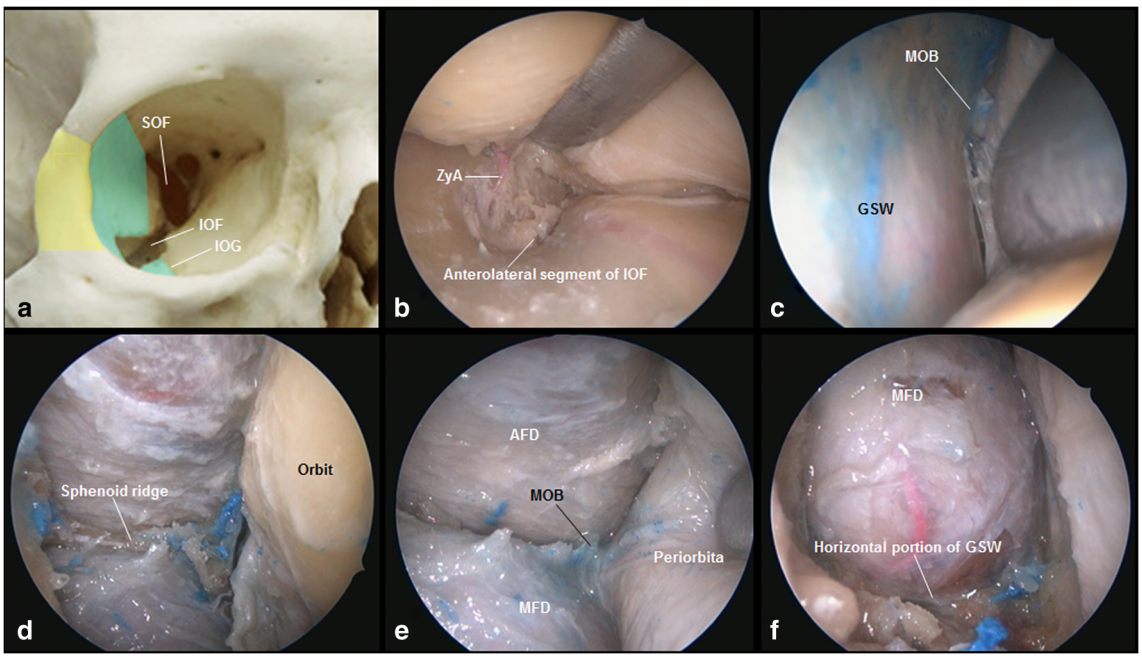


**Fig. 6** Drilling of the ocular surface of greater sphenoid wing (GSW) and lateral orbital rim osteotomy. **a** Planned range of craniectomy was colored with light green, and the extent of orbital rim osteotomy was colored with yellow. **b** Anterolateral segment of inferior orbital fissure (IOF) was transected to expose the ocular surface of GSW and orbital floor. **c** The meningo-orbital band (MOB), the anatomic landmark of lateral aspect of superior orbital fissure (SOF), was the medial boundary of bony drilling. **d**, **e** With progressive drilling posteriorly, the anterior fossa dura (AFD) above the orbital plate of frontal bone and the middle fossa dura (MFD) behind the ocular surface of GSW were identified. Full exposure of MOB was needed for subsequent middle cranial fossa dissection. **f** The lower boundary of bone drilling was the horizontal portion (infratemporal surface) of GSW. *IOG* infraorbital groove; *ZyA* zygomatic artery

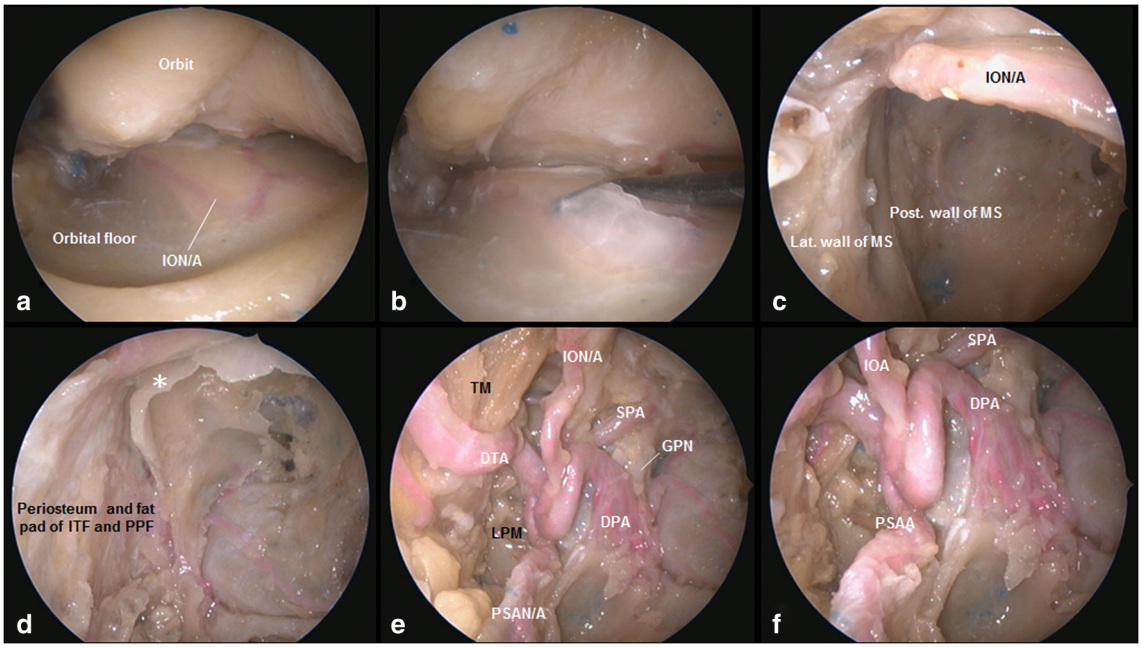


**Fig. 7** Entry to the maxillary sinus (MS) and exposure of pterygopalatine fossa (PPF) and infratemporal fossa (ITF). **a** The orbit was retracted superiorly to identify the infraorbital nerve along with infraorbital artery (ION/A) passing beneath the orbital floor. **b** Starting from medial to lateral, the orbital floor lateral to the ION/A was removed gently until reaching the lateral wall of MS. **c** Wide entrance into the MS was established. **d** Removing the posterior and lateral walls of MS exposed underlying periosteum and fat pad of ITF and PPF. Removal of the postero-superior corner (asterisk) of MS was necessary for subsequent mobilization of ION. **e** After dissecting underlying periosteum and fat pad, the contents of ITF and PPF were exposed. **f** Magnified endoscopic view of PPF. *DPA* descending palatine artery; *DTA* descending temporal artery; *GPN* greater palatine nerve; *Lat.* lateral; *LPM* lateral pterygoid muscle; *Post.* posterior; *PSAN/A* posterior superior alveolar nerve/artery; *SPA* sphenopalatine artery; *TM* temporalis muscle

get entry into the maxillary sinus (Fig. 7c). The posterior and lateral walls of the maxillary sinus were taken away to expose the underlying periosteum and fat pad of PPF and ITF (Fig. 7d). The orbitomaxillary segment of ION and pterygomaxillary fissure were the landmarks defining the boundary between the PPF and ITF. The PPF was located medially to them, and the ITF was located laterally. The posterosuperior corner of the maxillary sinus, anterior and lateral to the pterygopalatine segment of ION, was necessary to remove (Fig. 7d). This maneuver allowed subsequent medial mobilization of ION with establishing corridor for subsequent middle fossa drilling. Cutting the periosteum and removing the fat tissue exposed the contents of PPF and ITF (Fig. 7e, f). At first, the internal maxillary artery and its terminal branches were observed, including infraorbital, deep temporal, descending palatine, sphenopalatine, and posterior superior alveolar arteries. Next, the neural structures of the PPF, such as the sphenopalatine ganglion and the greater and lesser palatine nerves, were identified to be posterior to the sphenopalatine and descending palatine arteries. The lateral pterygoid muscle and temporalis muscle lied behind the vascular structures of ITF.

## Mobilization of ION with drilling of the infratemporal surface of GSW and pterygoid process

Tracing the orbitomaxillary segment and pterygopalatine segment of ION posteriorly led to identification of the foramen rotundum and MCF (Fig. 8a). Detachment of the upper head of lateral pterygoid muscle from bony origin, following a subperiosteal plane, and medial mobilization of ION exposed the infratemporal surface of GSW and pterygoid process widely (Fig. 8b). Drilling of the infratemporal surface of GSW along the base of lateral pterygoid plate would identify the foramen ovale and mandibular nerve (Fig. 8c).

## Exposure of the MCF, Meckel's cave, and lateral wall of cavernous sinus

The sphenoid bone situated between the foramen rotundum and the foramen ovale was drilled and flattened until exposure of the anterolateral triangle of the MCF exocranially (Fig. 8d). After that, the outer dura layer (dura propria) was peeled away from the inner meningeal layer from anterior to posterior. Tracing along the maxillary nerve and mandibular nerve posteriorly would lead to Gasserian ganglion and Meckel's cave

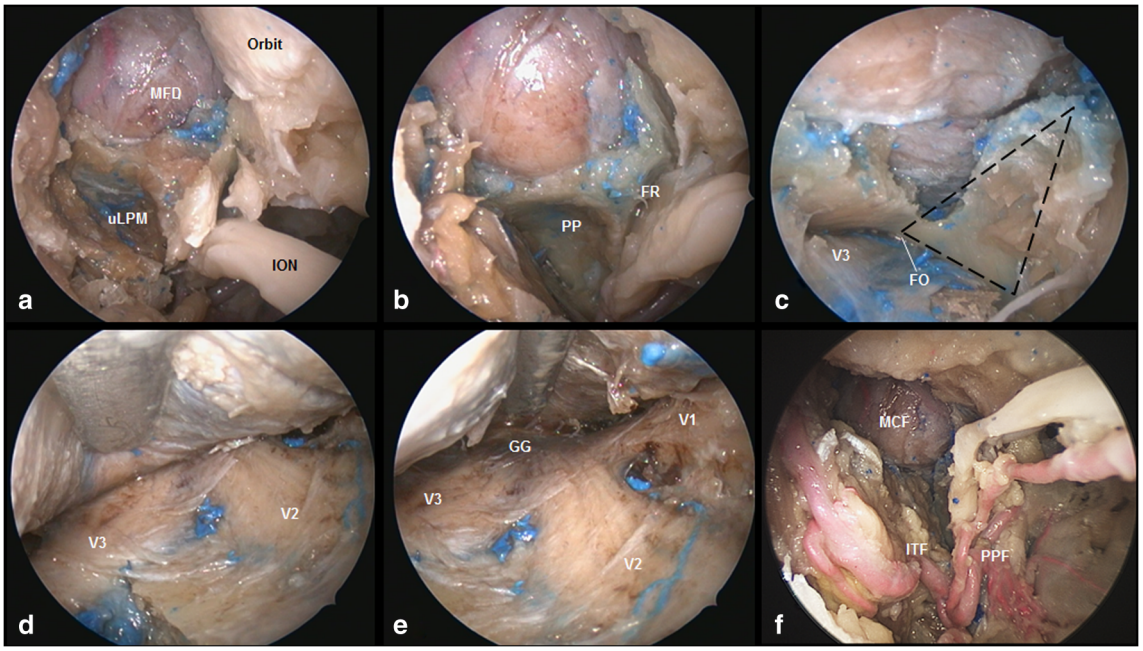


**Fig. 8** Exposure of middle cranial fossa (MCF) and Meckel's cave. **a** Tracing the infraorbital nerve (ION) posteriorly contributed to identify the foramen rotundum (FR) and MCF. **b** The base of pterygoid process (PP) was exposed widely by detaching the upper head of lateral pterygoid muscle (uLPM) from lateral pterygoid plate and medial mobilization of ION. **c** Drilling the upper end of lateral pterygoid plate led to recognize the foramen ovale (FO) and mandibular nerve (V3).The area of bone drilling was outlined by the black-dashed line. **d** FR was unroofed with exposure of the anterolateral triangle of MCF. **e** The dura propria was peeled away to expose the Gasserian ganglion (GG) and Meckel's cave. **f** The MCF, PPF, and ITF were exposed after completing the dissection. *V1* ophthalmic nerve; *V2* maxillary nerve

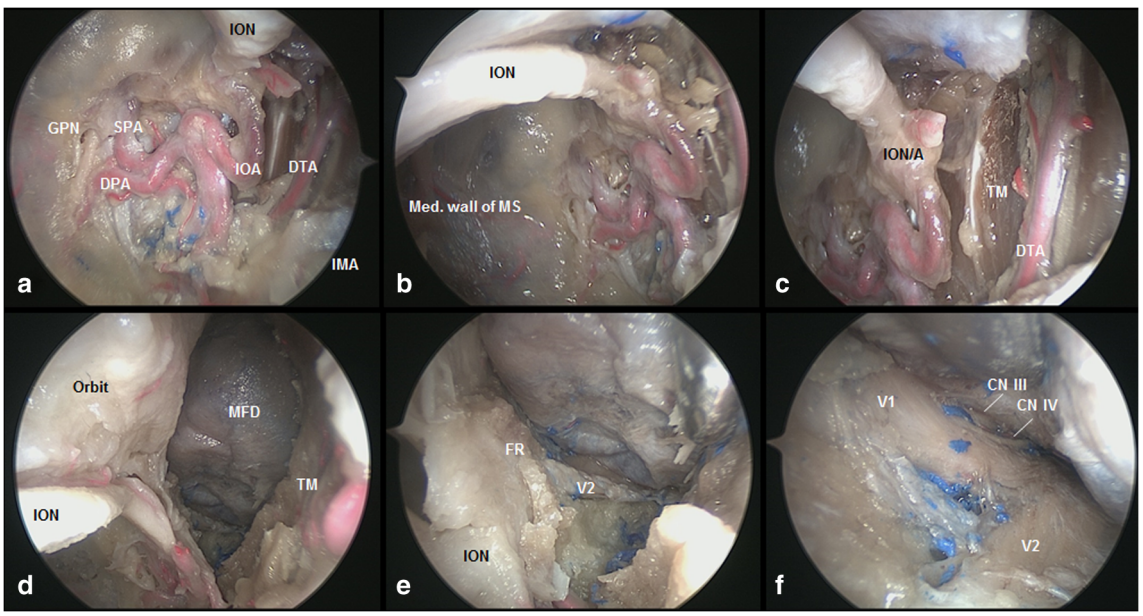


**Fig. 9** Exposed area of anterolateral skull base with a 30-degree endoscope in another cadaveric head (left side). **a** The neurovascular contents of infratemporal fossa (ITF) and pterygopalatine fossa (PPF). **b** Medial wall of the maxillary sinus (MS) formed the medial boundary of exposure. **c** Medial aspect of temporalis muscle limited lateral exposure of ITF. **d** Removing the postero-superior corner of MS allowed mobilization of orbitomaxillary and pterygopalatine segments of infraorbital nerve (ION). Following the ION posteriorly could identify the foramen rotundum (FR) and middle cranial fossa (MCF). **e** Pterygopalatine segment of ION passed through FR to become the maxillary nerve (V2). **f** The V2 passed in the lateral wall of cavernous sinus toward Gasserian ganglion. *CN III* oculomotor nerve; *CN IV* trochlear nerve; *DPA* descending palatine artery; *DTA* deep temporal artery; *GPN* greater palatine nerve; *IOA* infraorbital artery; *SPA* sphenopalatine artery; *TM* temporalis muscle; *V1* ophthalmic nerve

(Fig. 8e). Access to the lateral wall of the cavernous sinus was gained by continuing the dissection superiorly and medially. This dissection allowed direct visualization of three divisions of the trigeminal nerve as well as the oculomotor nerve and the trochlear nerve. The trochlear nerve was identified above the ophthalmic nerve, and the oculomotor nerve seated at the roof of cavernous sinus (Fig. 9e).

At the final stage of dissection, the PPF, ITF, MCF, and Meckel's cave were exposed simultaneously (Fig. 8f). In the end, the bony defect of orbital roof was reconstructed with custom-shaped titanium mesh, and the lateral orbital rim was repositioned with miniplates.

## Measured distances and exposed area of anterolateral skull base

The whole procedure was performed using a zero-degree endoscope. The 30-degree endoscope was mainly used to visualize the medial and lateral boundaries of the exposed area, especially the lateral wall of cavernous sinus. The exposed anterolateral skull base was a rectangular area (Fig. 10). The meningo-orbital band and frontal base constituted the upper limit of dissection. The inferior potion of the pterygoid process fusing with the posterior maxilla was the lower limit. The medial boundary of exposure was composed of the lateral wall of cavernous sinus superiorly and the medial wall of the maxillary sinus inferiorly, and the lateral boundary was temporalis muscle.

The mean distance from the reference point to the foramen rotundum was 45.0 ± 1.9 mm (range, 42–47 mm). The mean distance from the reference point to the foramen ovale was 55.7 ± 0.5 mm (range, 55–56 mm). The mean distance from the reference point to the Gasserian ganglion was 61.0 ± 1.6 mm (range, 59–63 mm). The working area for exposure of PPF and ITF was 426.1 ± 60.7 $mm^2$ (range, 383.3–406.5 $mm^2$). In comparison with the horizontal portion of GSW, the superior and inferior axes of area exposure were 22.3 ± 2.1 mm (range, 20–25 mm) and 20.5 ± 1.8 mm (range, 18–23 mm). With reference to the foramen rotundum, the medial and lateral axes of area exposure were 11.6 ± 1.1 mm (range, 10–13 mm) and 15.8 ± 1.6 mm (range, 13–17 mm). The results of measurements are shown in Table 1.

**Table 1** Results of measurements

| | Mean ± SD (mm) | Range (mm) |
|---|---|---|
| Distance | | |
| RP to FR | 45.00 ± 1.87 | 42–47 |
| RP to FO | 55.66 ± 0.471 | 55–56 |
| RP to GG | 61.00 ± 1.63 | 59–63 |
| RP to IOF | 21.75 ± 1.92 | 20–25 |
| IOF to FR | 42.00 ± 3.32 | 39–47 |
| Working space* ($mm^2$) | 426.14 ± 60.66 | 383.29–529.99 |
| Area of exposure | | |
| Medial axis | 11.75 ± 1.09 | 10–13 |
| Lateral axis | 15.75 ± 1.64 | 13–17 |
| Superior axis | 22.33 ± 2.05 | 20–25 |
| Inferior axis | 20.50 ± 1.80 | 18–23 |

*FR* foramen rotundum, *FO* foramen ovale, *GG* Gasserian ganglion, *IOF* infraorbital foramen, *RP* reference point

*The triangular area consisted of three points: reference point, foramen rotundum, and infraorbital foramen. The amount of space was calculated by measuring the distance between each point and using Heron's formula

## Discussion

Thanks to the flourishing development of endoscopic instruments and the knowledge of endoscopic anatomy, the endoscopic endonasal approach has become an alternative treatment for ventral skull base lesions. Beyond the natural boundary of sinonasal tract, lateral extension of the endoscopic endonasal approach allows minimally invasive access to the anterolateral skull base [10, 18, 21]. Several techniques regarding the endoscopic endonasal route to the anterolateral skull base have been addressed, and the most commonly used

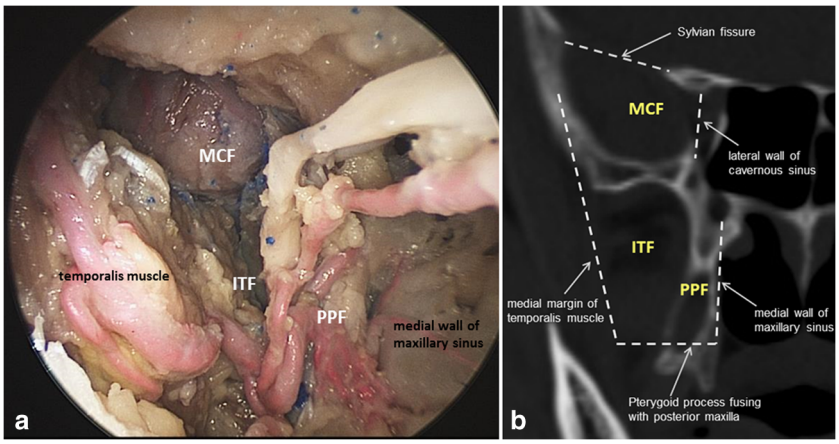


**Fig. 10** Endoscopic photography of exposed anterolateral skull base and corresponding computed tomographic image. **a** The middle cranial fossa (MCF), pterygopalatine fossa (PPF), and infratemporal fossa (F) were exposed widely. **b** Dashed lines illustrate the limits and boundaries of dissection in the coronal plane of posterior wall of the maxillary sinus

one being the endoscopic endonasal transmaxillary transpterygoid approach [17, 18, 21]. Establishing the surgical corridor of the endoscopic endonasal approach to the anterolateral skull base needs an inferior-to-superior and medial-to-lateral trajectory. In order to achieve adequate exposure of anterolateral skull base, it requires extensive bone drilling near the cavernous sinus, sacrificing the Vidian nerve and the pterygopalatine ganglion, and cauterization of the internal maxillary artery. Therefore, these maneuvers may result in eye redness and nose dryness and carry the potential risk of internal carotid artery injury and ION damage [5, 23, 26]. To overcome these limitations, the endoscopic sublabial transmaxillary transpterygoid approach is considered as another choice of minimally invasive surgery to anterolateral skull base [34, 35]. Although sparing dissection in close proximity to cavernous sinus and internal carotid artery, sacrificing the contents of PPF is still required.

The transorbital neuroendoscopic surgery, first described by Moe et al., has been announced as an alternative treatment for paramedian skull base lesions of anterior and middle fossae [20, 22, 25, 27]. Because eTOA provides one novel pathway to skull base, recent studies have focused on expanded applications of eTOA to different areas of interest [3, 6, 12, 15]. Owing to the IOF forming relay station between the orbit and surrounding fossae, removing the bony structures surrounding the IOF in order to gain entry into anterolateral skull base is the main speculation of this study. The IOF is a narrow space located between the posterior two thirds of lateral orbital wall and the orbital floor. The whole length of IOF, from the anterior aspect of maxillary strut to the most anterolateral aspect of IOF, is divided into posteromedial, middle, and anterolateral segments [4, 9, 32]. The posteromedial segment, from the maxillary strut to the posterior border of infraorbital groove, communicates with pterygopalatine fossa. The middle segment, the width of the infraorbital groove at the IOF, connects the orbits to the infratemporal fossa [36]. The anterolateral segment, from the anterior border of infraorbital groove to the most anterolateral aspect of IOF, provides direct access to temporal fossa [4, 32].

On the basis of this cadaveric study, the study results support the hypothesis that the eTOA through IOF is a feasible, novel, and minimally invasive access to make a wide exploration of anterolateral skull base. The combination of preseptal approach and retrocanthal approach with additional lateral cantholysis is used as the choice of eyelid incision. This is because the preseptal approach provides direct access to the orbital floor and the retrocanthal approach is recommended for selected lesion over the lateral orbital apex and MCF [25]. Initially, the entry plane of eTOA is coplanar with the orbital floor. Then, widening the lateral two thirds of IOF superiorly and laterally by drilling the ocular surface of GSW and orbital rim osteotomy not only allows exposure of MCF and Meckel's cave, behind the orbit, but also establishes space for surgical maneuverability. After that, widening the IOF inferiorly and laterally by removal of maxilla surrounding IOF, including orbital surface lateral to the infraorbital groove, posterior and lateral walls of the maxillary sinus, allows exposure of PPF and ITF, below the orbit. Finally, the goal of drilling the infratemporal surface of GSW and pterygoid process is to remove the anatomical barrier located between the MCF and ITF.

A variety of benign and malignant neoplasms may involve the anterolateral skull base, and sometime, the lesions occupy not only one confined region. Thus, how to choose the most suitable surgical approach to target lesion involving multiple compartments of anterolateral skull base is challenging to clinicians. By the result of this study, the eTOA through IOF provides a possible resolution and selection to manage this clinical difficulty. Comparing with the endoscopic endonasal transpterygoid approach providing medial-to-lateral and inferior-to-superior trajectory, the eTOA through IOF establishes corridor with lateral-to-medial direction and a wide range of surgical maneuverability in the sagittal plane. Thus, the direction of attack can be adjusted according to different areas of interest. In brief, the major benefit of this design is avoidance of sinonasal trauma and confined exposure of target area limited by internal carotid artery and cranial nerves.

During the whole procedure, the ION is a reliable landmark to guide the direction of dissection. The importance of ION in the endonasal transmaxillary approach has been addressed by Elhadi et al. [14]. With elevation of orbital content, the orbitomaxillary segment of ION is immediately identified below the orbital floor. Following the course of orbitomaxillary segment of ION posteriorly leads to infraorbital groove and retromaxillary space. The infraorbital groove at the IOF contains the transition of orbitomaxillary segment and pterygopalatine segment of ION. Removing the posterior wall and postero-superior corner of the maxillary sinus is needed to identify and free the pterygopalatine segment of ION. The maxillary nerve passing through the foramen rotundum to Gasserian ganglion can guide bone drilling of the infratemporal surface of GSW until exposure of the anterolateral triangle of MCF.

This study demonstrates that it is feasible to get a wide exposure of anterolateral skull base using the eTOA through IOF without sacrificing any critical neurovascular structure. However, the orbitomaxillary and pterygopalatine segments of ION are at possible risk of damage secondary to manipulation. It may cause numbness of face. The posterior and middle superior alveolar nerves and the posterior superior alveolar artery are also at risk of damage while removing the posterior and lateral walls of the maxillary sinus with resulting anesthesia of upper teeth. Apart from this, primary reconstruction of orbital floor is recommended to prevent postoperative enophthalmos and hypoglobus [1, 11]. This cadaveric study is a laboratory investigation with normal anatomy. Our results

do not exactly represent the pathological changes in real surgery, and further clinical studies are needed to confirm its clinical practicality.

## Conclusions

This cadaveric study describes a novel approach to anterolateral skull base using eTOA through IOF. For mass lesions occupying more than one specific region of anterolateral skull base, it provides an alternative minimally invasive access.

**Funding** This work was supported by the Tri-Service General Hospital of Taiwan's Medical Research Project (TSGH-C104-078 and TSGH-C107-071).

### Compliance with ethical standards

**Conflict of interest** The authors declare that they have no conflict of interest.

**Ethical approval** All procedures performed in studies involving human participants were in accordance with the ethical standards of the institutional and/or national research committee and with the 1964 Helsinki Declaration and its later amendments or comparable ethical standards.

**Informed consent** Informed consent was obtained from all individual participants included in the study.

## References

1. Allen RC (2016) The evolving role of the oculoplastic surgeon in skull base surgery. Curr Opin Ophthalmol 27(5):402–407
2. Almeida JP, Omay SB, Shetty SR et al (2018) Transorbital endoscopic eyelid approach for resection of sphenoorbital meningiomas with predominant hyperostosis: report of 2 cases. J Neurosurg 128(6):1885–1895
3. Almeida JP, Ruiz-Trevino AS, Shetty SR, Omay SB, Anand VK, Schwartz TH (2017) Transorbital endoscopic approach for exposure of the sylvian fissure, middle cerebral artery and crural cistern: an anatomical study. Acta Neurochir 159(10):1893–1907
4. Aziz KM, Froelich SC, Cohen PL, Sanan A, Keller JT, van Loveren HR (2002) The one-piece orbitozygomatic approach: the MacCarty burr hole and the inferior orbital fissure as keys to technique and application. Acta Neurochir 144(1):15–24
5. Cebula H, Kurbanov A, Zimmer LA et al (2014) Endoscopic, endonasal variability in the anatomy of the internal carotid artery. World Neurosurg 82(6):e759–e764
6. Chen HI, Bohman LE, Loevner LA, Lucas TH (2014) Transorbital endoscopic amygdalohippocampectomy: a feasibility investigation. J Neurosurg 120(6):1428–1436
7. Dallan I, Di Somma A, Prats-Galino A et al (2017) Endoscopic transorbital route to the cavernous sinus through the meningo-orbital band: a descriptive anatomical study. J Neurosurg 127(3):622–629
8. Dallan I, Sellari-Franceschini S, Turri-Zanoni M et al (2018) Endoscopic transorbital superior eyelid approach for the management of selected spheno-orbital meningiomas: preliminary experience. Oper Neurosurg (Hagerstown) 14(3):243–251
9. De Battista JC, Zimmer LA, Theodosopoulos PV, Froelich SC, Keller JT (2012) Anatomy of the inferior orbital fissure: implications for endoscopic cranial base surgery. J Neurol Surg B Skull Base 73(2):132–138
10. de Lara D, Ditzel Filho LF, Prevedello DM et al (2014) Endonasal endoscopic approaches to the paramedian skull base. World Neurosurg 82(6 Suppl:S121–S129
11. DeMonte F, Tabrizi P, Culpepper SA, Suki D, Soparkar CN, Patrinely JR (2002) Ophthalmological outcome after orbital entry during anterior and anterolateral skull base surgery. J Neurosurg 97(4):851–856
12. Di Somma A, Andaluz N, Cavallo LM et al (2018) Endoscopic transorbital superior eyelid approach: anatomical study from a neurosurgical perspective. J Neurosurg 129(5):1203–1216
13. Di Somma A, Andaluz N, Cavallo LM et al (2018) Endoscopic transorbital route to the petrous apex: a feasibility anatomic study. Acta Neurochir 160(4):707–720
14. Elhadi AM, Zaidi HA, Yagmurlu K et al (2016) Infraorbital nerve: a surgically relevant landmark for the pterygopalatine fossa, cavernous sinus, and anterolateral skull base in endoscopic transmaxillary approaches. J Neurosurg 125(6):1460–1468
15. Ferrari M, Schreiber A, Mattavelli D et al (2016) The inferolateral transorbital endoscopic approach: a preclinical anatomic study. World Neurosurg 90:403–413
16. Fisch U, Fagan P, Valavanis A (1984) The infratemporal fossa approach for the lateral skull base. Otolaryngol Clin N Am 17(3):513–552
17. Harvey RJ, Sheehan PO, Debnath NI, Schlosser RJ (2009) Transseptal approach for extended endoscopic resections of the maxilla and infratemporal fossa. Am J Rhinol Allergy 23(4):426–432
18. Hofstetter CP, Singh A, Anand VK, Kacker A, Schwartz TH (2010) The endoscopic, endonasal, transmaxillary transpterygoid approach to the pterygopalatine fossa, infratemporal fossa, petrous apex, and the Meckel cave. J Neurosurg 113(5):967–974
19. Janecka IP, Sen CN, Sekhar LN, Arriaga M (1990) Facial translocation: a new approach to the cranial base. Otolaryngol Head Neck Surg 103(3):413–419
20. Jeon C, Hong CK, Woo KI et al Endoscopic transorbital surgery for Meckel's cave and middle cranial fossa tumors: surgical technique and early results. J Neurosurg 1:1–10. https://doi.org/10.3171/2018.6.JNS181099
21. Kassam AB, Gardner P, Snyderman C, Mintz A, Carrau R (2005) Expanded endonasal approach: fully endoscopic, completely transnasal approach to the middle third of the clivus, petrous bone, middle cranial fossa, and infratemporal fossa. Neurosurg Focus 19(1):E6
22. Kong DS, Young SM, Hong CK et al (2018) Clinical and ophthalmological outcome of endoscopic transorbital surgery for cranioorbital tumors. J Neurosurg [epub ahead of print:1–9. https://doi.org/10.3171/2018.3.JNS173233
23. Labib MA, Prevedello DM, Carrau R et al (2014) A road map to the internal carotid artery in expanded endoscopic endonasal approaches to the ventral cranial base. Neurosurgery 10(Suppl 3):448–471
24. Landreneau FE, Mickey B, Coimbra C (1998) Surgical treatment of cerebrospinal fluid fistulae involving lateral extension of the sphenoid sinus. Neurosurgery 42(5):1101–1104
25. Moe KS, Bergeron CM, Ellenbogen RG (2010) Transorbital neuroendoscopic surgery. Neurosurgery 67(3 Suppl Operative):ons16–ons28
26. Pinheiro-Neto CD, Fernandez-Miranda JC, Prevedello DM, Carrau RL, Gardner PA, Snyderman CH (2013) Transposition of the pterygopalatine fossa during endoscopic endonasal transpterygoid approaches. J Neurol Surg B Skull Base 74(5):266–270

27. Ramakrishna R, Kim LJ, Bly RA, Moe K, Ferreira M Jr (2016) Transorbital neuroendoscopic surgery for the treatment of skull base lesions. J Clin Neurosci 24:99–104
28. Raza SM, Donaldson AM, Mehta A, Tsiouris AJ, Anand VK, Schwartz TH (2014) Surgical management of trigeminal schwannomas: defining the role for endoscopic endonasal approaches. Neurosurg Focus 37(4):E17
29. Reynolds JM, Tomkinson A, Grigg RG, Perry CF (1998) A Le Fort I osteotomy approach to lateral sphenoid sinus encephalocoeles. J Laryngol Otol 112(8):779–781
30. Schwartz TH, Fraser JF, Brown S, Tabaee A, Kacker A, Anand VK (2008) Endoscopic cranial base surgery: classification of operative approaches. Neurosurgery 62(5):991–1002
31. Sekhar LN, Schramm VL Jr, Jones NF (1987) Subtemporal-preauricular infratemporal fossa approach to large lateral and posterior cranial base neoplasms. J Neurosurg 67(4):488–499
32. Shimizu S, Tanriover N, Rhoton AL Jr, Yoshioka N, Fujii K (2005) MacCarty keyhole and inferior orbital fissure in orbitozygomatic craniotomy. Neurosurgery 57(1 Suppl):152–159
33. Shin SS, Gardner PA, Stefko ST, Madhok R, Fernandez-Miranda JC, Snyderman CH (2011) Endoscopic endonasal approach for nonvestibular schwannomas. Neurosurgery 69(5):1046–1057
34. Truong HQ, Sun X, Celtikci E et al (2018) Endoscopic anterior transmaxillary "transalisphenoid" approach to Meckel's cave and the middle cranial fossa: an anatomical study and clinical application. J Neurosurg 130(1):227–237
35. Yagmurlu K, Mooney MA, Almefty KK et al (2018) An alternative endoscopic anterolateral route to Meckel's cave: an anatomic feasibility study using a sublabial transmaxillary approach. World Neurosurg 114:134–141
36. Zimmer LA, Hart C, Theodosopoulos PV (2009) Endoscopic anatomy of the petrous segment of the internal carotid artery. Am J Rhinol Allergy 23(2):192–196